Aerotecnica Missili & Spazio (2022) 101:7–15
https://doi.org/10.1007/s42496-022-00106-9

ORIGINAL ARTICLE

# Evaluation of Satellite's Point-Ahead Angle Derived from TLE for Laser Communication

**Riccardo Lazzaro**[1] · **Carlo Bettanini**[1]

Received: 1 November 2021 / Revised: 10 January 2022 / Accepted: 12 January 2022 / Published online: 2 February 2022


**Abstract**
Advances in lasers, optics and electronics for Satellite's optical communication are opening the possibility of very high performance near Earth space links with data rate up to several Gbps. Being the divergence of the laser beam typically of tens of $\mu$rad, an extremely high precision pointing is needed to correctly establish and maintain data optical link. In particular, the relative motion between the satellite and the ground station shall be accurately evaluated to estimate how to correct pointing angles for future orbital locations. This correction is made via a point-ahead mirror (PAM) mechanism, which deviates the laser beam by an angle called point-ahead angle (PAA). The purpose of this paper is evaluate the possibility of accurately estimate the point-ahead angle in advance using the two-line elements sets for the orbiting satellite, which are available before the ground station overpass. The study evaluated TLE-based orbital evolution of Sentinel-6 satellite, comparing the results with the high precision data obtained by laser ranging from the crustal dynamics data information system (CDDIS). The maximum error observed between the estimated and measured point-ahead angles was less than 1 $\mu$rad, demonstrating the possibility of this point-ahead correction technique for LEO orbiting satellites.

**Keywords** Laser communication · Satellite · TLE · Laser ranging · Point-ahead angle

## 1 Introduction

The creation of an optical link with an orbiting satellite relies on the localization of the receiver in the sky via a beacon laser of sufficient beam divergence to account for the uncertainty of the search area; once the signal is detected by the target terminal, narrower circular beams are initiated from both terminals using the first acquired position as a reference for acquisition, tracking and pointing. The main challenge in establishing the end-to-end link is, therefore, an accurate knowledge in advance of the satellite's orbital state to correctly point the scanning beam. One technique to refine coarse orbit prediction by numerical propagation is high precision orbit estimation using laser ranging, but this operation requires additional on-board hardware and the presence of several ground station worldwide to provide accurate tracking [1].

It is also possible to determine the satellite's position and orbit with optical observation from the ground station, correcting the pointing errors in the early stages of the pass [2].

Once the satellite is correctly acquired, the fine tracking can start; in this phase, a very high precision pointing of the laser must be obtained, since its narrowness is extremely small. This can be achieved with a series of fine sensors and mirrors, which continually correct the pointing in a closed-loop control system [3]. To achieve the required level of accuracy in controlling the dis-alignment induced by satellite-ground station relative motion, dedicated algorithms based on Kalman filtering are usually implemented in the optical units control software [4].

A simpler and less hardware demanding approach can be based on target position estimation based on numerical orbit prediction using publicly available two-line element sets; the estimated orbital parameters are generally affected by an error depending on set generation time [5] and orbit type [6] but may be efficiently used for LEO satellites as will be shown in this paper comparing the results with the ones of accurate orbit determination with satellite laser ranging.

✉ Riccardo Lazzaro
riccardo.lazzaro@outlook.it

[1] Department of Industrial Engineering, University of Padova, via Venezia 1, Padua, Italy

**Table 1** Orbital parameters of Sentinel-6

| sma (km) | inc (°) | ecc | RAAN (°) | AOP (°) | TA (°) | Epoch (mjd) |
|---|---|---|---|---|---|---|
| 7721.6 | 66.09 | 4.2E−4 | 164.7 | 13.2 | 346.9 | 59460.511887 |

**Table 2** Ground station coordinates in ECEF

| Latitude (°) | Longitude (°) | Altitude (km) |
|---|---|---|
| 40.649 | 16.705 | 0.537 |

**Table 3** Satellite's drag parameters

| Mass (kg) | Area ($m^2$) | Cd |
|---|---|---|
| 1100 | 10 | 2.2 |

## 2 Orbit Propagation and Point Ahead Angle Calculation

The initial state vector of the satellite is obtained using standard conversion of the available TLE sets [7]; propagation is then performed using GMAT[1] software considering EGM-96 gravity model and MSISE-90 atmospheric model with variable F10.7 and Ap and adding the following perturbations: Luni-solar perturbations, Solar radiation pressure and tide effects.

The considered satellite is Sentinel-6 and the optical ground station (OGS) is Matera Laser Ranging Observatory; the orbital parameters of the satellite before the propagation in ECI reference system and ground station position in ECEF reference system are reported in Tables 1 and 2. The satellite's drag parameters considered for the propagation are shown in Table 3, the attitude mode is assumed to be nadir-pointing. Since the total propagation time does not exceed one or two days, the effect of atmospheric drag is small. Therefore, more precise parameters are not investigated in this analysis.

Because of the finite speed of light, the up-link and down-link beams will be separated by an angle called point ahead angle (PAA). This angle can be easily calculated once the orbital parameters of the satellite are obtained.

Starting from the TLE set, the orbit is obtained considering smoothed SGP4 perturbation using Matlab [8], then propagated with GMAT and the PAA for a specific link is calculated. The PAA for the same link is also obtained using ILRS' consolidated prediction format (CPF) file [9] for the same satellite, comparing the two results and analyzing the difference.

The Sentinel-6 CPF dataset based on laser ranging measurements is obtained from the online archives of the crustal dynamics data information system (CDDIS) [10].

To evaluate the PAA, the propagation time from ground to the satellite is calculated using

$$t_p = \frac{R}{c}, \tag{1}$$

where $R$ is the slant range and $c$ the speed of light. The PAA is then

$$\theta_{PA} = 2\,\frac{V_t}{c}\ (\text{rad}), \tag{2}$$

where $V_t$ is the relative tangential velocity [11].

The effect of atmospheric refraction of the laser has been previously analyzed (e.g. [2]) and, since it does not affect the calculation of the PAA, it is not included in this paper. Furthermore, the speed of light is considered constant in our calculation given that the error introduced by its variation through the atmosphere is negligible.

To define the PAA starting from the tracking coordinates (azimuth $\alpha$, elevation $\beta$ and slant range $\rho$), the commonly used point ahead angles in the tracking reference system are $\alpha_{PA}$ and $\beta_{PA}$ [3]:

$$\alpha_{PA}(t) = \frac{d\alpha(t)}{dt} * \frac{2\rho(t)}{c} \approx \frac{2[\alpha(t+dt) - \alpha(t)]\,\rho(t)}{c\,dt}, \tag{3}$$

$$\beta_{PA}(t) = \frac{d\beta(t)}{dt} * \frac{2\rho(t)}{c} \approx \frac{2[\beta(t+dt) - \beta(t)]\,\rho(t)}{c\,dt}. \tag{4}$$

The azimuth-elevation-range reference system presents a singularity point at an elevation of 90°; at this point the azimuth is not defined and its derivative tends to infinite affecting the calculation of $\alpha_{PA}$.

However, the needed PAA for the actual correction performed by the point-ahead mirror (PAM) can be obtained using a simple trigonometric relation that bypass the mathematical issues with the above-mentioned equation [3]:

$$\alpha_{PAM}(t) = \alpha_{PA}(t)\,\cos[\beta(t)], \tag{5}$$

$$\beta_{PAM}(t) = \beta_{PA}(t). \tag{6}$$

Finally, the point ahead angle referred to the PAM is then obtained using

[1] NASA General Mission Analysis Tool

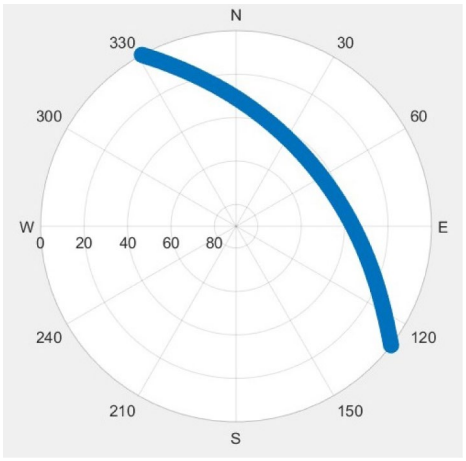


(a) skyplot

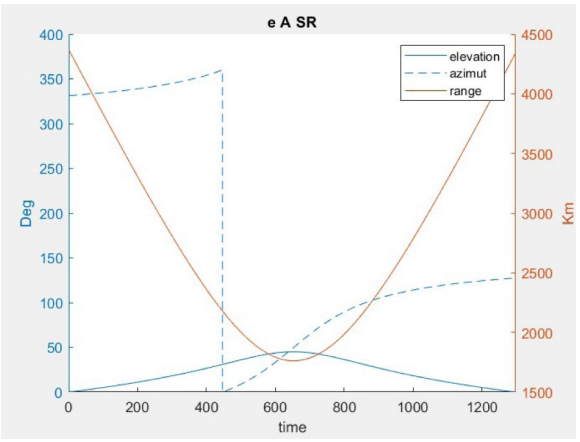


(b) elevation azimuth range

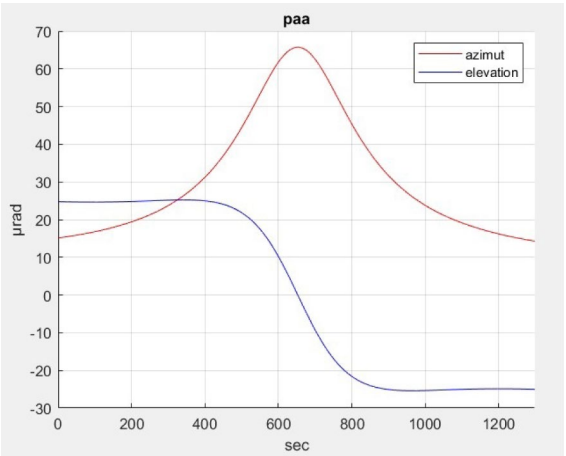


(c) Azimuth and elevation PAA

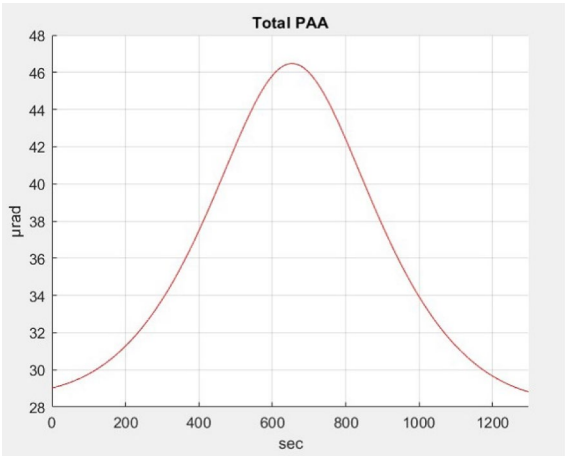


(d) $\theta_{PAM}$

**Fig. 1** Pass 1

$$\theta_{\mathrm{PAM}}(t) = \sqrt{[\alpha_{\mathrm{PAM}}(t)]^2 + [\beta_{\mathrm{PAM}}(t)]^2}. \tag{7}$$

## 3 Results of PAA Angle Calculation Using TLE Sets

This section presents the results for three representative passes of Sentinel-6 over the OGS. The first one is a medium elevation pass of approximately 45°, while the second a relative high pass of nearly 70°. The last one is a very high elevation pass of slightly less than 90°, from which it can be observed the behavior of the PAA near the singularity point.

The results are visualized in four different plots. The first one represents the azimuth and elevation angles in a sky-plot over observation station (Fig. 1a). The second plot reports the time variation during the pass of the same angles, along with the values of satellite range (Fig. 1b).The considered starting time for the pass ($t = 0$) is set as $\beta = 0$.

The last two plots show the evolution of the point-ahead angles, decomposed in elevation ($\beta_{\mathrm{PA}}$) and azimuth ($\alpha_{\mathrm{PA}}$) by Eqs. 3 and 4 and then recombined in $\theta_{\mathrm{PAM}}$ using Eqs. 5–7 (Fig. 1c, d). This method is applied for all three passes and during the whole track (Fig. 2).

A selection of representative data during each passage for the considered parameters is also reported in the accompanying Tables 4, 5, 6.

### 3.1 Pass 1

See Fig. 1 and Table 4.

### 3.2 Pass 2

See Fig. 2 and Table 5.

**Table 4** Pass 1

| Time (s) | El (°) | Az ° | PAA(μrad) | $\alpha_{PA}$(μrad) | $\beta_{PA}$(μrad) |
|---|---|---|---|---|---|
| 100 | 5.18 | 334.51 | 29.77 | 16.78 | 24.64 |
| 200 | 11.13 | 338.86 | 31.27 | 19.41 | 24.81 |
| 300 | 18.17 | 344.90 | 33.77 | 23.74 | 25.14 |
| 400 | 26.57 | 354.00 | 37.48 | 31.25 | 24.97 |
| 500 | 35.99 | 8.83 | 42.07 | 44.44 | 21.84 |
| 600 | 43.69 | 33.23 | 45.82 | 61.78 | 10.19 |
| 652 | 45.02 | 49.65 | 46.47 | 65.74 | − 0.00 |
| 700 | 43.93 | 64.51 | 45.98 | 62.53 | − 9.28 |
| 800 | 36.44 | 89.52 | 42.39 | 45.33 | − 21.61 |
| 900 | 26.92 | 104.76 | 37.75 | 31.65 | − 25.08 |
| 1000 | 18.39 | 114.02 | 33.92 | 23.76 | − 25.34 |
| 1100 | 11.22 | 120.08 | 31.28 | 19.12 | − 25.03 |
| 1200 | 5.17 | 124.35 | 29.66 | 16.20 | − 24.88 |

### 3.3 Pass 3

See Fig. 3 and Table 6

Elaboration of the data allows to underline that the maximum value of PAA is obtained at the point of maximum elevation, where the relative tangential velocity is highest. When approaching this orbital point the $\theta_{PA}$ value reaches nearly the same expected value for every pass as reported in Table 7.

The third pass shows the behavior of the point-ahead angles in the 90 ° pass case. In this situation, the azimuth angle is subject to a nearly instantaneous shift from the arriving value of 210–30° (Fig. 3a). This causes the derivative of $\alpha$ to rapidly increase (Fig. 3a), reflecting this behavior on $\alpha_{PA}$ (Fig. 3c) that present a narrow spike with the maximum point being over 8900 μrad (Table 6). Nevertheless,

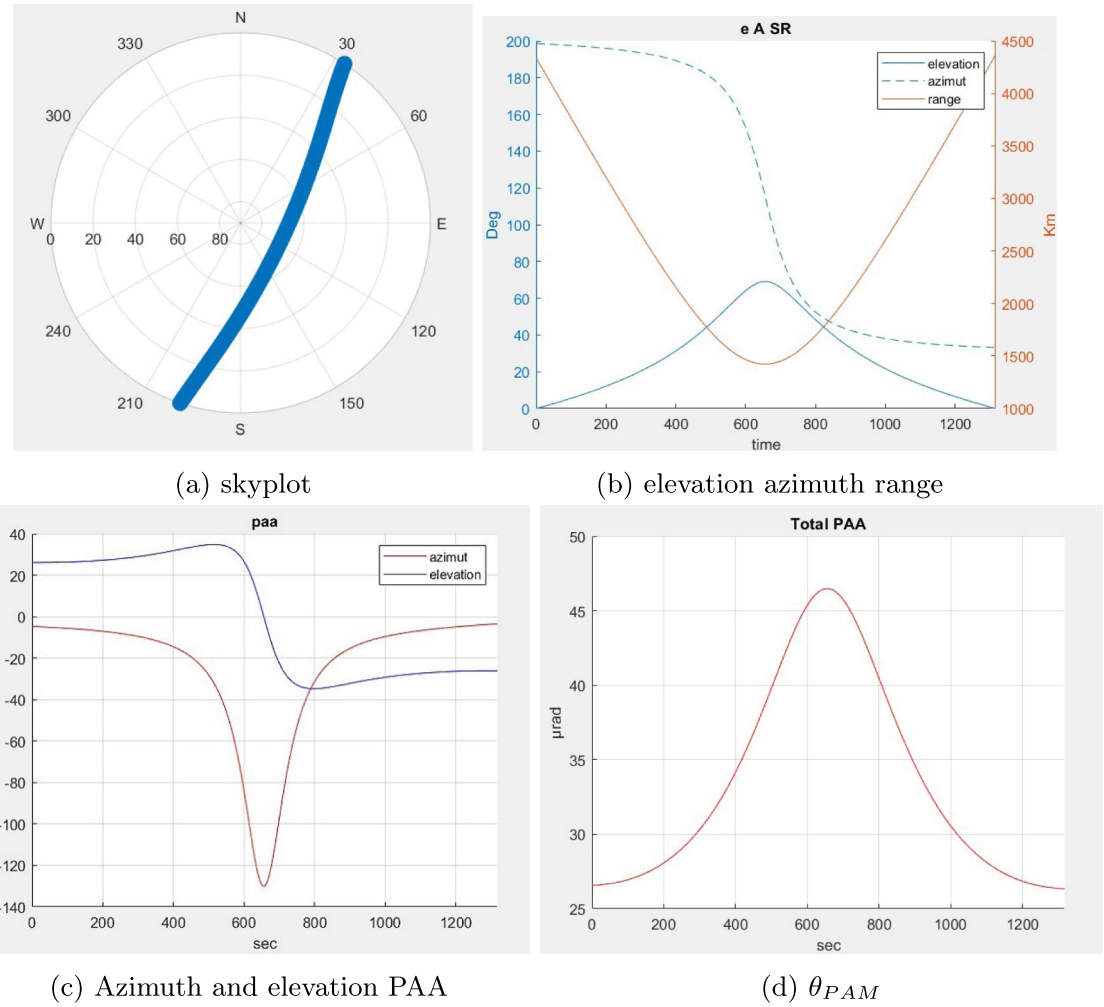


(a) skyplot (b) elevation azimuth range

(c) Azimuth and elevation PAA (d) $\theta_{PAM}$

**Fig. 2** Pass 2

**Table 5** Pass 2

| Time (s) | El ° | Az ° | PAA(μrad) | $\alpha_{PA}$(μrad) | $\beta_{PA}$(μrad) |
|---|---|---|---|---|---|
| 100 | 5.56 | 197.50 | 26.95 | – 5.64 | 26.36 |
| 200 | 12.17 | 195.94 | 28.08 | – 7.07 | 27.21 |
| 300 | 20.41 | 193.52 | 30.32 | – 9.53 | 28.97 |
| 400 | 31.31 | 189.29 | 34.17 | – 14.53 | 31.83 |
| 500 | 46.24 | 180.25 | 39.81 | – 28.17 | 34.72 |
| 600 | 64.08 | 152.92 | 45.37 | – 84.26 | 26.50 |
| 655 | 69.06 | 115.46 | 46.49 | – 130.07 | – 0.01 |
| 700 | 65.82 | 84.39 | 45.74 | – 96.97 | – 22.68 |
| 800 | 48.39 | 52.57 | 40.45 | – 31.22 | – 34.73 |
| 900 | 32.99 | 42.55 | 34.62 | – 15.28 | – 32.16 |
| 1000 | 21.73 | 38.09 | 30.54 | – 9.59 | – 29.21 |
| 1100 | 13.26 | 35.67 | 28.10 | – 6.72 | – 27.33 |
| 1200 | 6.52 | 34.21 | 26.84 | – 4.93 | – 26.39 |
| 1300 | 0.86 | 33.29 | 26.37 | – 3.66 | – 26.11 |

using Eqs. 5 and 7, the $\theta_{\mathrm{PAM}}$ reaches again the same expected value (Fig. 3d).

## 4 Error of TLE Prediction vs Pseudo-observation Data (CPF files)

To estimate the accuracy of the results, we compared the PAA derived from the TLEs with those obtained using the CPF files [10], which have a prediction uncertainty of less than 10 m [9], so they are often considered as pseudo-observations.

The point-ahead angles are calculated again using the procedure described in Sect. 2, but using the interpolated data from the CPF files as the starting point. These results are then compared to those obtained before using the TLE; the difference is reported in the following figures, both for a low elevation pass (40 °) (Fig. 4) and an high elevation pass

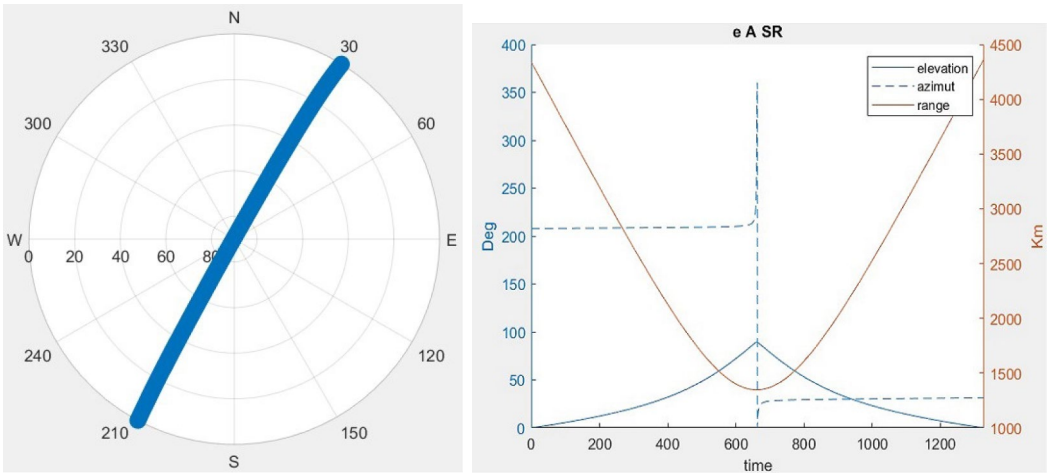


(a) skyplot

(b) elevation azimuth range

(c) Azimuth and elevation PAA

(d) $\theta_{PAM}$

**Fig. 3** Pass 3

**Table 6** Pass 3

| Time (s) | El ° | Az ° | PAA(μrad) | $\alpha_{PA}$(μrad) | $\beta_{PA}$(μrad) |
|---|---|---|---|---|---|
| 300 | 20.68075 | 208.6256 | 29.60516 | 0.789336 | 29.59595 |
| 400 | 32.02004 | 208.9076 | 33.27584 | 0.778638 | 33.26929 |
| 500 | 48.38865 | 209.2822 | 38.93901 | 0.91918 | 38.93423 |
| 600 | 72.19072 | 210.1155 | 45.00499 | 2.902777 | 44.99623 |
| 659 | 89.34013 | 236.071 | 46.49742 | 1808.184 | 41.53167 |
| 660 | 89.58296 | 254.7127 | 46.5384 | 4521.721 | 32.73726 |
| 661 | 89.70321 | 299.9984 | 46.47794 | 8973.062 | − 0.29388 |
| 662 | 89.57821 | 344.636 | 46.42112 | 4464.9 | − 32.9444 |
| 663 | 89.33415 | 2.887955 | 46.45798 | 1790.012 | − 41.5821 |
| 700 | 78.71322 | 27.96506 | 45.84945 | 6.629812 | − 45.8311 |
| 800 | 53.25397 | 29.3323 | 40.36 | 1.119546 | − 40.3544 |
| 900 | 35.41589 | 29.81324 | 34.32299 | 0.981009 | − 34.3137 |
| 1000 | 23.18972 | 30.2086 | 30.21516 | 1.125863 | − 30.1974 |
| 1100 | 14.27272 | 30.58886 | 27.84631 | 1.358728 | − 27.8152 |

**Table 7** Max $\theta_{PAM}$

| | Max elevation (°) | Min range (km) | Max $\theta_{PAM}$ (μrad) |
|---|---|---|---|
| Pass 1 | 45.02 | 1423 | 46.47 |
| Pass 2 | 69.06 | 1494 | 46.49 |
| Pass 3 | 89.70 | 1346 | 46.47 |

(80 °) (Fig. 5). The interpolation process of the CPF causes a minor numerical uncertainty that is reported as a band in the graphs.

It may be noted that the maximum error in the point-ahead angle does not exceed 1μrad even for the highest elevation pass (Fig. 5) and that the error remains very close to zero for most of the pass. This suggests the PAA data obtained trough the TLE being quite as accurate as the one by pseudo observations and may be successfully used for tracking a LEO satellite.

Considering absolute pointing angles (azimuth and elevation), the difference between the pointing angles obtained from TLEs and from CPF is reported in Fig. 6.

For these angles, the accuracy obtained through TLE elaboration is much lower, since the relative error reaches 10–20 mdeg in the low elevation pass and up to 100 mdeg in the high one. The absolute error in comparison with the pseudo observation data is therefore well above the divergence of the laser beam and so the TLE-based data cannot be used to perform a reliable pointing.

The main cause for such discrepancy can be observed comparing the time evolution of pointing angles obtained with the two methods. In Fig. 7, the elevation and azimuth time profiles during the pass are plotted, in red for the TLE-based data and in blue for CPF. Focusing on the red square, it can be seen that the red curve reaches 360 ° in azimuth slightly before the blue one. This time bias between the two datasets is within the order 0.1 s and accounts for the main contribution to the relative error in the pointing angles.

This error is caused by the non-perfect accuracy in the initial orbital position provided by the TLE. This imprecision is implicit in the TLE data and is caused mainly by the inaccuracy in the data collection network [8]. It is not clear how to asses the magnitude of the error [5], many studies have tried to estimate the precision of the TLE by comparison with GPS and laser ranging data (e.g. [6, 12]) and the results vary upon the satellite's orbit. For a LEO satellite the initial orbital position error is estimated to be in the order of 1–2 km *at-epoch*.

This initial error then propagates over time, resulting in a loss of accuracy after a few days. For this reason the TLE prediction should be updated with the latest data available,

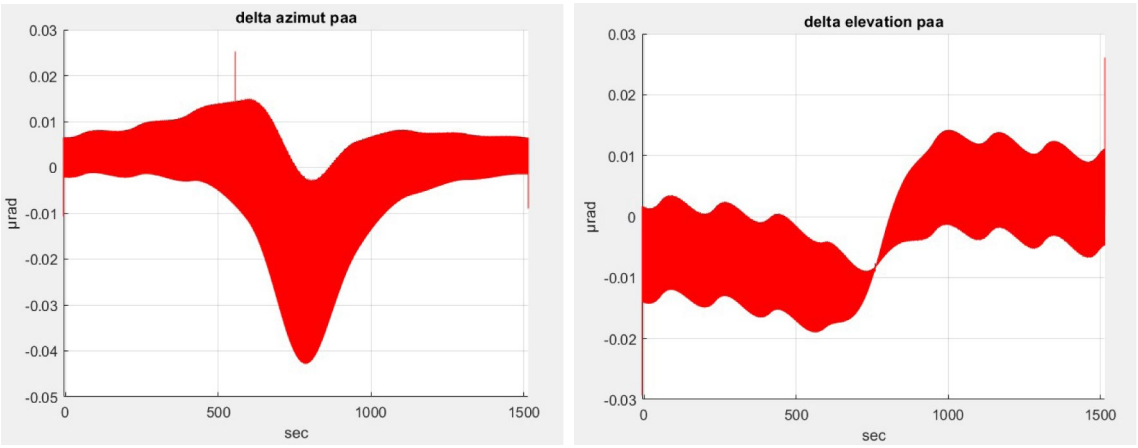


(a) Azimuth PA error (b) Elevation PA error

**Fig. 4** Point ahead error—low elevation pass

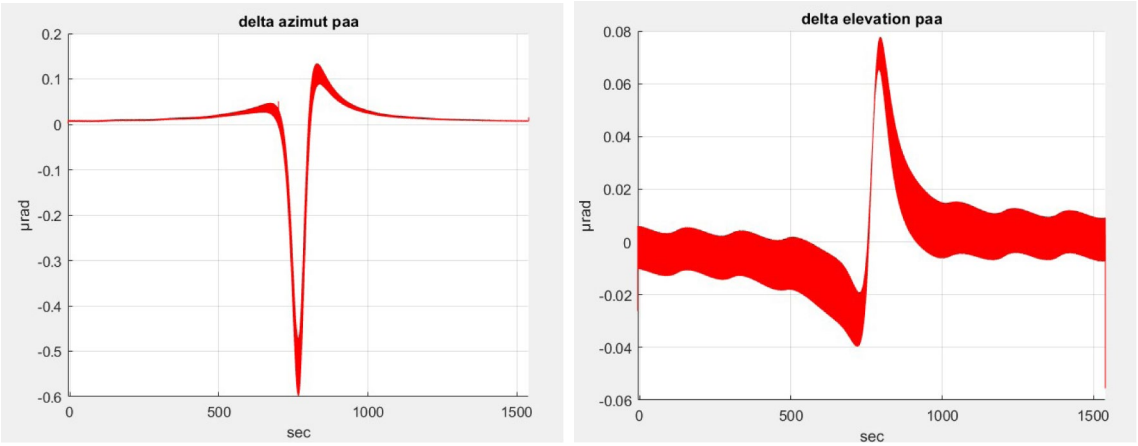


(a) Azimuth PA error (b) Elevation PA error

**Fig. 5** Point ahead error—high elevation pass

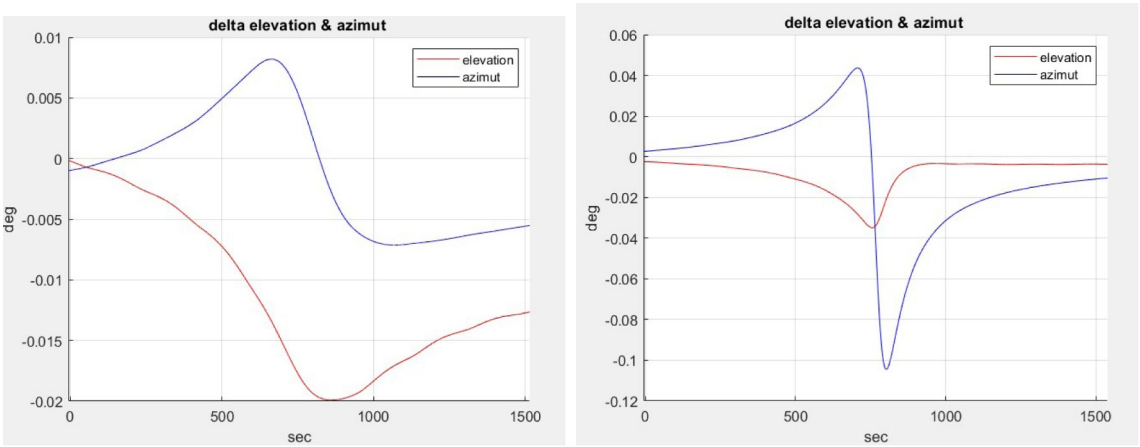


(a) Low elevation pass (b) High elevation pass

**Fig. 6** Azimuth and elevation error

and for a high precision analysis the TLE should not be more than 1 or 2 days old.

The orbital position error can be decomposed into along and cross track directions. The along track error is responsible for the high time bias seen in the previous analysis. Figure 8a shows an example of the orbital error evolution within a day, defined as the magnitude of the error vector between the TLE and CPF orbital predictions. As expected, the orbital error is around 1 km at the start of the simulation and grows over time, reaching up to 4 km after 1 day.

To analyze the relation between the orbital error and the PAA, a variable time bias is introduced by hand in the TLE data and the error of the $\theta_{\mathrm{PAM}}$ between CPF and TLE is visualized in the following figure (Fig. 8b) for several passes of different maximum elevation.

From these considerations, it can be observed that the PAA error, for a very high elevation pass and an extremely high time bias, approaches 7 μrad at the point of maximum elevation. In this, the laser link can potentially experience a short period of unstable communication when the satellite passes near the zenith. For all practical cases, with time biases below 0.5 s and passes with a maximum elevation of less than 80 degrees, the error remains below 1 μrad. For this reason, the TLE should not be older than 1 or 2 days, to contain the time bias.

In the case of a satellite being at low altitude, where the atmospheric drag perturbations becomes significant, the consideration of using the latest TLE available becomes even more important.

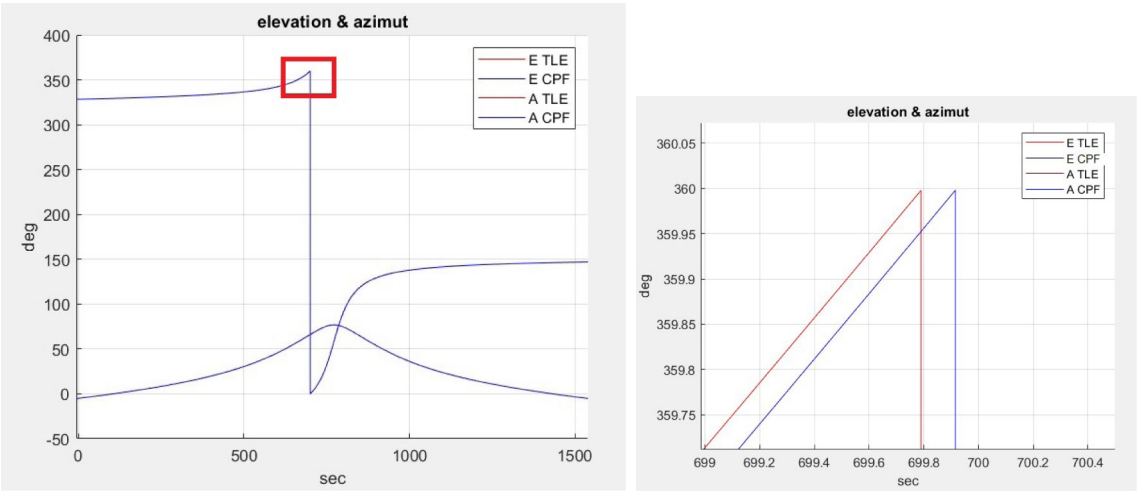


(a) Elevation & Azimuth during pass (b) Red square focus

**Fig. 7** CPF-TLE time bias

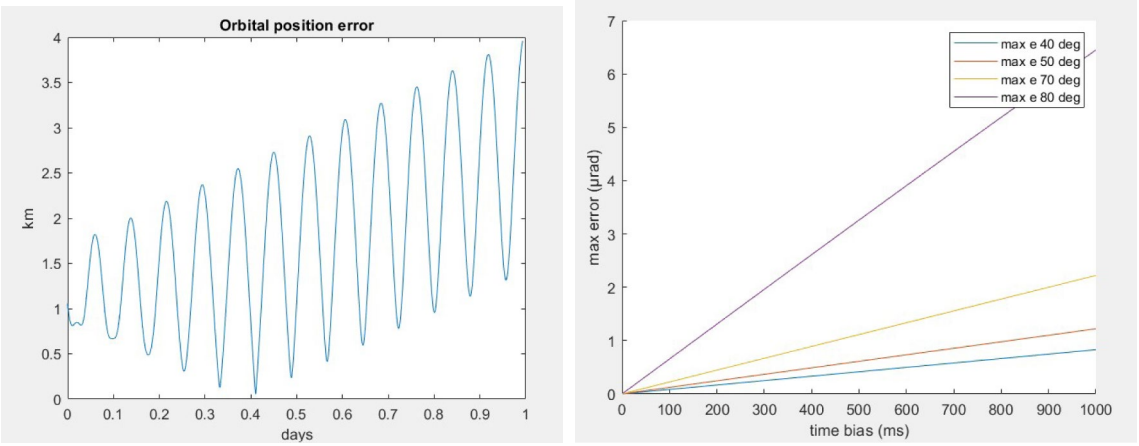


(a) Orbital position error evolution (b) $\theta_{PAM}$ error - time bias

**Fig. 8** Orbital position error—$\theta_{PAM}$ error

## 5 Conclusion

Analyzing the results of orbital propagation of Sentinel-6, high accuracy in the PAA can be obtained through the used TLE and accurate numerical propagation of perturbed orbit. The angles obtained can reliably be used in tracking to correct for the point-ahead misalignment, with only the exception of the 90 ° elevation pass where the tracking angles are not well defined.

The obtained maximum error of the PAA relative to the CPF's pseudo observation is in fact lower 1 μrad for all practical cases, as seen in Figs. 4 and 5, far less than the laser beam's divergence.

On the other side, the accuracy obtained in azimuth and elevation angles using TLE-based propagation is not high enough to guarantee satellite tracking from the ground station, since the error in the both elevation and azimuth angles is substantially more than the divergence of the beacon.

Therefore, to successfully set an end-to-end optical link between a satellite and a ground station, it is necessary to rely on direct measurement (optical or laser ranging) to track satellite position and orbit. Afterwards, it is possible to correct the PA angle using the values calculated from the TLE.

## Declarations

**Conflict of interest** On behalf of all the authors, the corresponding author states that there is no conflict of interest.



## References

1. Iqbal, F., Kirchner, G., Koidl, F., Leitg, E.: Laser back scatter: limitation to higher repetition rate [khz] satellite laser ranging system. Geodesy Geodyn. **12**, 48–53 (2021)
2. Liu, N.: Acquisition and tracking strategies for satellite to ground optical communication systems, Master's thesis, Ryerson University (2018). https://doi.org/10.32920/ryerson.14645112.v1
3. Han, X., Yong, H., Xu, P., Wang, W., Yang, K., Xuev, H., Cai, W., Ren, J., Peng, C., Pan, J.: Point-ahead demonstration of a transmitting antenna for satellite quantum communication. Opt. Express **26**, 17044–17055 (2018)
4. Zhang, F., Ruan, P., Han, J.: Point ahead angle prediction based on Kalman filtering of optical axis pointing angle in satellite laser communication. Opt. Rev. **27**, 447–454 (2020)
5. Kelso, T.: Norad two-line element set format, Tech. rep. (2000) https://www.celestrak.com/NORAD/documentation/tle-fmt.aspf
6. Xiao-li, X., Yong-qing, X.: Study on the orbit prediction errors of space objects based on historical TLE data. Chin. Astron. Astrophys. **43**, 563–578 (2019)
7. Hoots, R., Roehrich, L.: Models for propagation of NORAD element sets. In: Technical report, aerospace defense command peterson afb co office of astrodynamics (2020)
8. Vallado, D.: Fundamental of astrodynamics and applications, 4th edition, space technology library - Microcosm Press (2013)
9. Noll, C.: The crustal dynamics data information system: a resource to support scientific analysis using space geodesy. Adv. Space Res. **45**(12), 1421–1440 (2010). https://doi.org/10.1016/j.asr.2010.01.018
10. Slr sentinel-6 cpf data: Online archives of the crustal dynamics data information system (cddis), Tech. rep., NASA Goddard Space Flight Center, Greenbelt, MD, USA. https://cddis.nasa.gov/archive/slr/cpf_predicts_v2/current/ (2021). Accessed Sep 2021
11. Maral, G., Bousquet, M., Sun, Z.: Satellite Communications Systems, 6th edn. Wiley, Hoboken (2020)
12. Ly, D., Lucken, R., Giolito, D.: Correcting TLEs at epoch: application to the GPS constellation. J. Space Saf. Eng. **7**(3), 302–306 (2020)